

Morphometric analysis in gamma-ray astronomy using Minkowski functionals:

III. Sensitivity increase via a refined structure quantification

M. A. Klatt^{1,2,3} * and K. Mecke^{2,3}

¹ Karlsruhe Institute of Technology (KIT), Institute of Stochastics, Englerstr. 2, 76131 Karlsruhe, Germany

² Institut für Theoretische Physik, Universität Erlangen-Nürnberg, Staudtstr. 7, 91058 Erlangen, Germany

³ Erlangen Centre for Astroparticle Physics, Universität Erlangen-Nürnberg, Erwin-Rommel-Str. 1, 91058 Erlangen, Germany

Received ... / Accepted ...

ABSTRACT

Aims. We pursue a novel morphometric analysis to detect sources in very-high-energy gamma-ray counts maps by structural deviations from the background noise without assuming any prior knowledge about potential sources. The rich and complex structure of the background noise is characterized by Minkowski functionals from integral geometry. By extracting more information out of the same data, we aim for an increased sensitivity.

Methods. In the first two papers, we derived accurate estimates of the joint distribution of all Minkowski functionals. Here, we use this detailed structure characterization to detect structural deviations from the background noise in a null hypothesis test. We compare the analysis of the same simulated data with either a single or all Minkowski functionals.

Results. The joint structure quantification can detect formerly undetected sources. We show how the additional shape information leads to the increase in sensitivity. We explain the very unique concepts and possibilities of our analysis compared to a standard counting method in gamma-ray astronomy, and we present in an outlook further improvements especially for the detection of diffuse background radiation and generalizations of our technique.

Key words. Methods: data analysis – Methods: statistical – Techniques: image processing – Gamma rays: diffuse background

1. Morphometric source detection in gamma-ray astronomy

The morphometric analysis quantifies the complex structural information that is contained in the background noise in ground-based Very-High Energy (VHE) gamma-ray astronomy. We thus quantify the shape of sky maps without any assumption about potential sources (Klatt et al. 2012; Göring et al. 2013).

The Minkowski functionals from integral geometry can comprehensively and robustly quantify the complex shape provided by spatial data (Schneider & Weil 2008; Mantz et al. 2008; Schröder-Turk et al. 2010, 2011, 2013). They allow for an efficient data analysis and a sensitive hypothesis test. Because of their versatility, they cannot only check for specific structures or arrangements but can detect any structural deviation from the expected background. In other words, by characterizing the shape of a noisy sky-map more information can be taken out of the same data without assuming prior knowledge about the source.

This is in contrast to the common null hypothesis test by Li & Ma (1983) that only uses the total number of counts but no further geometric information, which might be especially valuable for the analysis of extended sources or diffuse VHE emissions Aharonian et al. (2006a, 2007, 2006b). It is also in contrast to full likelihood fits of models to the mea-

sured data of high-energy gamma-ray telescopes (Mattox et al. 1996; Atwood et al. 2009), which strongly depend on the model and on the a-priori knowledge about the sources.

The methods and concepts in this article are in principle applicable to any random field and any spatial data to detect inhomogeneities or other structural deviations. It could, for example, be interesting for medical data sets, e.g., in tumor recognition (Canuto et al. 2009; Larkin et al. 2014; Arfelli et al. 2000; Michel et al. 2013), for geospatial data and raster data in earth science (Stonebraker et al. 1993), in image and video analysis, where a fast analysis for the detection of objects is needed (Borg et al. 2005; Yilmaz et al. 2006; Quast & Kaup 2011), or in the related field of pattern recognition (Jain et al. 2000; Theodoridis & Koutroumbas 2009). However, the technique is especially interesting for very high energy (VHE) gamma-ray astronomy, where faint extended signals are overlaid by strong background noise (Buckley et al. 2008). Especially, for short observation times and low statistics, that is, when an increase in sensitivity is most needed, the advantage of additional structural information should be most effective: the excess in the number of counts might not be significant because of the strong fluctuations of a Poisson distribution relative to the small mean value. However, the improbable spatial arrangement of the fluctuations can eventually lead to the detection of the source.

* e-mail: michael.klatt@kit.edu

In astronomy, the Minkowski functionals are already used as probes of non-Gaussianity in the cosmic microwave background (Schmalzing et al. 1999; Novikov et al. 2000; Gay et al. 2012; Ducout et al. 2013; Novaes et al. 2014), to characterize nuclear matter in supernova explosions (Schuetrumpf et al. 2013, 2015), and to investigate the large-scale structure of the universe (Mecke et al. 1994; Colombi et al. 2000; M. Kerscher et al. 2001; Kerscher et al. 2001; Wiegand et al. 2014).

In the first two papers of this series, we introduced the morphometric analysis to gamma-ray astronomy and derived accurate estimates of the structure distribution of the background. Here, we apply this refined shape analysis to simulated data and demonstrate how the additional geometric information can lead to a strong increase in sensitivity.

In Sec. 2, we shortly summarize the most important steps of the morphometric analysis. In Sec. 3, we demonstrate the increase in sensitivity via a refined structure quantification. By analyzing the same data simultaneously by all three Minkowski functionals instead of a simple structure characterization, the compatibility with the background structure can decrease by 14 orders of magnitude, that is, the probability to find such a fluctuation in the background is 10^{-19} instead of 10^{-5} . Formerly undetected sources can thus eventually be detected, which depends of course on the shape of the source whether there is a structural deviation or not.

The morphometric analysis is then compared in Section 4 to a standard null hypothesis test in gamma-ray astronomy. The comparison depends both on the shape of the source and on the experimental details. An advantage of the morphometric analysis is that it is rather independent of the size of the scan window. Moreover, we discuss an example for which there is no significant excess in the total number of counts, but the source can still be detected because of the additional structural information.

Section 5 contains a summary of the results and a conclusion. An outlook to further possible extensions is presented in Sec. 6.

In the appendix A, we introduce a new test statistic, which combines different thresholds. This allows, for example, for a better detection of diffuse radiation¹.

2. The statistical significance of structural deviations

In the first paper of this series, we explained in detail the structure characterization of a counts map itself using Minkowski functionals. Moreover, we rigorously defined the null hypothesis test that (globally) detects statistical significant deviations in the background noise. The most important steps were shortly repeated in the second paper. For a better readability, we also here repeat the definition of the test statistics.

The counts map is first turned into a black-and-white image by thresholding, that is, all pixels with a number of counts larger or equal a given threshold are set to black (otherwise white). The Minkowski functionals of the resulting two-dimensional black-and-white image are given by the area A , perimeter P , and Euler characteristic χ of the black

pixels (Schröder-Turk et al. 2011). The last functional is a topological quantity. It is given by the number of clusters minus the number of holes.

Given a measured count map, we compute for each threshold ρ a triplet (A, P, χ) of Minkowski functionals.

The null hypothesis is that there are only background signals, that is, we assume that all events are randomly, independently, and homogeneously distributed over the field of view. The first two papers demonstrated how detector effects that distort the homogeneity can be corrected for. The number of counts follow a Poisson distribution and they are independent for different bins of equal size. Their expectation λ is the background intensity.

For each given threshold ρ , the probability distribution $\mathcal{P}(A, P, \chi)$ of the Minkowski functionals can be determined under the null hypothesis that there are only background signals, as explained in the second paper of this series. The joint probability distribution of the Minkowski functionals sensitively characterizes the “shape of the background noise”. It allows to define a null hypothesis that detects statistical significant deviations from the background morphology. Following Neyman & Pearson (1933), we defined the *compatibility* C of a measured triplet (A, P, χ) with the null hypothesis:

$$C(A, P, \chi) = \sum_{\mathcal{P}(A_i, P_i, \chi_i) \leq \mathcal{P}(A, P, \chi)} \mathcal{P}(A_i, P_i, \chi_i). \quad (1)$$

For convenience, we then defined the *deviation strength* \mathcal{D} as the logarithm of this likelihood value:

$$\mathcal{D}(A, P, \chi) := -\log_{10} C(A, P, \chi); \quad (2)$$

the larger the deviation strength, the larger is the statistical significance of the structural deviation from the background intensity, more precisely. We reject the null hypothesis of a pure background measurement if the deviation strength is larger than 6.2, which corresponds to the common criterion of a 5σ deviation.

3. Sensitivity increase via structure characterization

We demonstrated that the morphometric analysis is a promising and innovative spatial data analysis in the first paper of this series, where we also discussed in an outlook its potentials and advantages. We achieved an accurate characterization of the complex structure of the background noise in the second paper. Here, we will show how our refined shape analysis can indeed lead to a strong increase in sensitivity. The advanced hypothesis test based on all three Minkowski functionals can detect sources that remain undetected if only a single functional is used.

The deviation strength $\mathcal{D}(A)$ w.r.t. only the area is the following called “simple deviation strength”, while the deviation strength $\mathcal{D}(A, P, \chi)$ w.r.t. the complete characterization via all three Minkowski functionals is called “joint deviation strength”.

3.1. Examples of Minkowski sky maps

In order to compare the simple to the joint deviation strength, we define a test pattern including sources of different sizes and different integrated fluxes and thus simulate count maps, see Fig. 1(a).

¹ Parts of this article are from the PhD thesis of one of the authors (Klatt 2016).

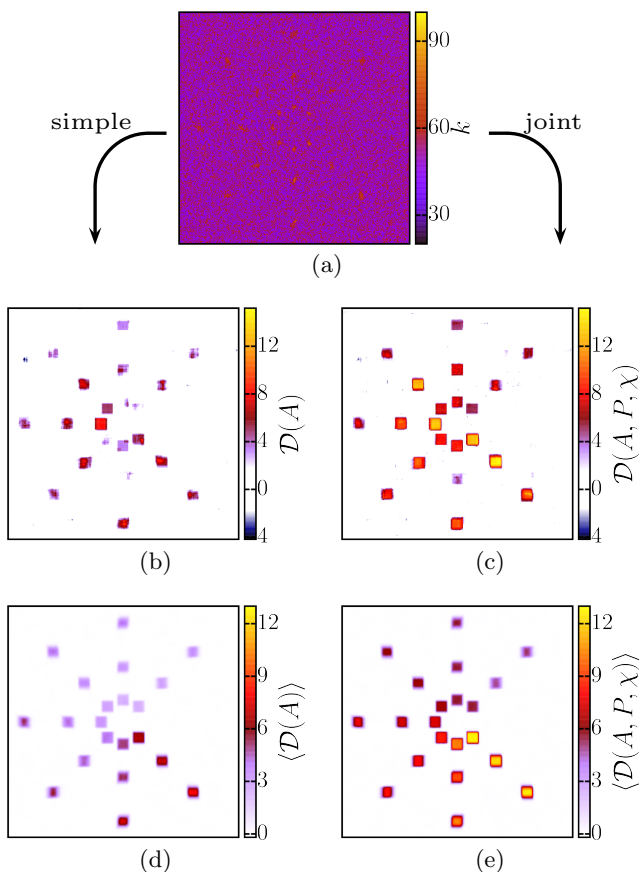


Fig. 1. Strong sensitivity increase via joint structure characterization: (a) simulated counts map including sources of different sizes and different integrated fluxes; the same count map is first analyzed by (b) a Minkowski sky map using the simple deviation strength, i.e., only area, then, using (c) the joint deviation strength, i.e., all Minkowski functionals; formerly undetected sources are now detected. For a more systematic comparison also averages of 100 Minkowski sky maps w.r.t. (d) only the area and (e) all three Minkowski functionals are shown.

The count map is both analyzed by a Minkowski sky map of the simple and the joint deviation strength, see Figs. 1(b) and 1(c), respectively. Note that the sources can be chosen much weaker than in the test pattern in the first paper of this series. This is because the 15×15 sliding window uses more statistics than the small 5×5 sliding windows. Therefore, weaker sources can be detected against strong background noise.

To demonstrate that the increased sensitivity is not a coincidence of a single fluctuation but a true grain in sensitivity due to the additional structure information, we plot the average of 100 Minkowski sky maps based on different simulations, see Figs. 1(d) and 1(e). The joint deviation strengths $\mathcal{D}(A, P, \chi)$ are on average distinctly larger than the simple deviation strengths $\mathcal{D}(A)$ analyzing the very same data.

The simple deviation strength can be expected to be significant only for the strongest sources. However, using all Minkowski functionals to characterize the structure of the counts maps, i.e., extracting more information from the same data, all sources are detected (where the faint sources

are, of course, in single simulations sometimes detected or not depending on statistical fluctuations). This confirms the initial idea to improve the sensitivity via an improved structure characterization.

The test pattern in Fig. 1 also reveals another advantage of the morphometric analysis. Differently large sources can be detected with the same scan window size in contrast to the standard counting method. This is discussed in more detail in Section 4.

In an outlook based on time-consuming calculations of the DoS of a 20×20 , we found that the sensitivity increase gets even stronger with further increasing window sizes. If necessary, the analysis can be extended to such window sizes.

3.2. Systematic analysis of increase in sensitivity

The test pattern in Fig. 1 demonstrates that using the joint structure characterization allows for detecting formerly undetected sources by taking additional morphometric information into account. Of course, an increase in sensitivity can only be achieved if there actually is an additional non-trivial shape information within the scan-window, more precisely, if the shape of the source is structured on the length scale of the sliding window.

If any morphometric approach is to analyze a completely uniform offset in the background intensity, i.e., a Poisson random field with a different intensity $\lambda' > \lambda$, the result must be less significant than for a simple method based only the total number of counts. This is simply because the additional structural information is in perfect accordance with the background model and the only difference is a different total number of counts.

In Fig. 1, the simple and joint deviation strengths are systematically compared to each other for differently shaped sources:

1. a true point source which is smaller than a pixel,
2. a uniform offset in the background intensity,
3. and a Gaussian shaped source.

Between 0.75 and 7.5 million counts maps (15×15) are simulated using the same intensity profile but different integrated fluxes. For each count map, both the simple and the joint deviation strength are determined. Given a simple deviation strength $\mathcal{D}(A)$, the conditional frequency $f[\mathcal{D}(A, P, \chi) | \mathcal{D}(A)]$ of the joint deviation strength $\mathcal{D}(A, P, \chi)$ is determined, i.e., for all cells with a simple deviation strength $\mathcal{D}(A)$ the empirical probability density function of the joint deviation strength $\mathcal{D}(A, P, \chi)$ is computed. The result is plotted using a color scale in Fig. 1. The black diagonal line indicates what would be equal values of simple and joint deviation strength. The vertical and horizontal black lines depict the null hypothesis criterion for the simple or joint deviation strength, respectively.

Not even the strongest true point source in these simulations would have been detected by a simple counting method because the source signals are suppressed by the large additional background. In contrast to this, even the simple deviation strength uses additional information the dependence on the threshold ρ and can thus, e.g., detect a single pixel with an exceptional high number of counts because of a unlikely black pixel at very high thresholds. This advantage in being more independent on the system size is discussed in more detail below in Section 4.

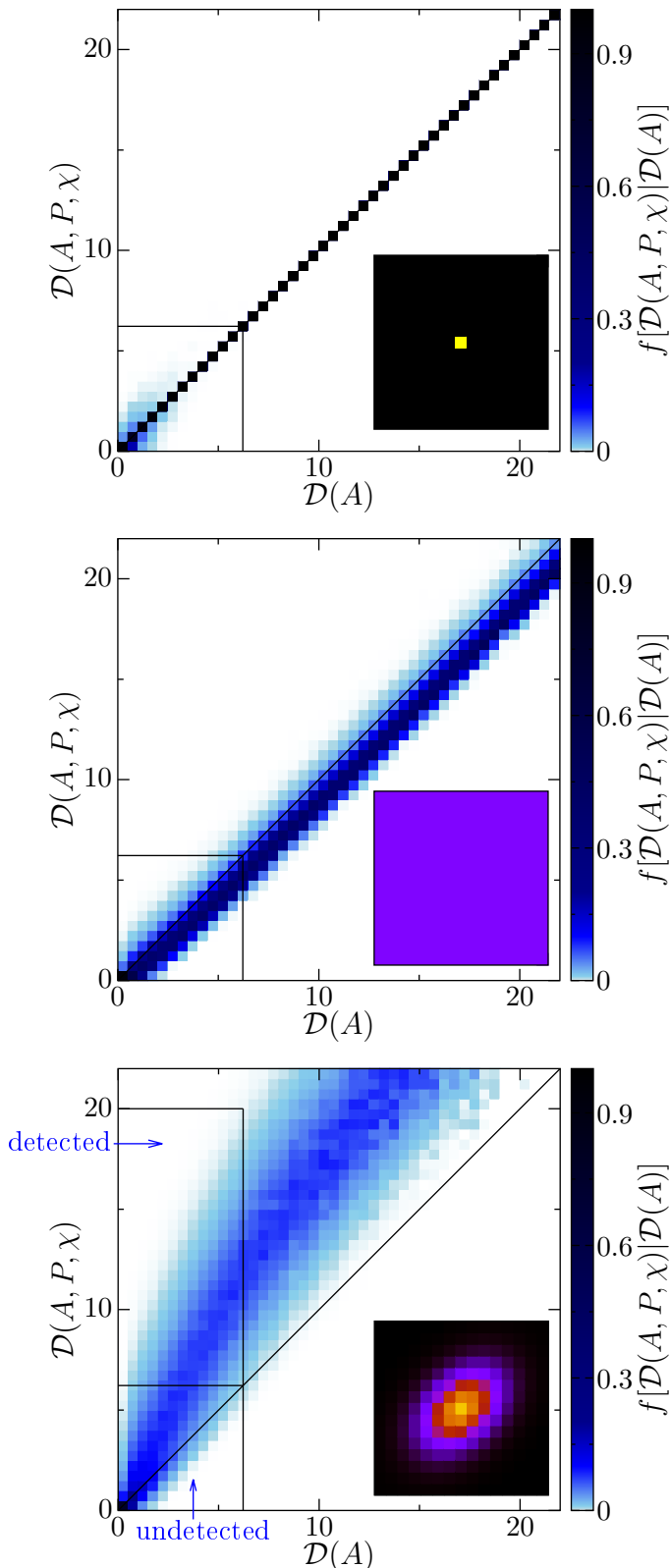


Fig. 2. The sensitivity increase, comparing simple to joint deviation strengths, depends on the source shape. Given $\mathcal{D}(A)$, the color code shows the frequency f of $\mathcal{D}(A, P, \chi)$ for the same counts map. We analyze (top) a true point source that is smaller than a pixel, (center) a uniform offset compared to the background intensity, and (bottom) an extended source with a nontrivial shape within the scan window, i.e., a strong gradient in the intensity. The insets show the intensity profiles of the sources.

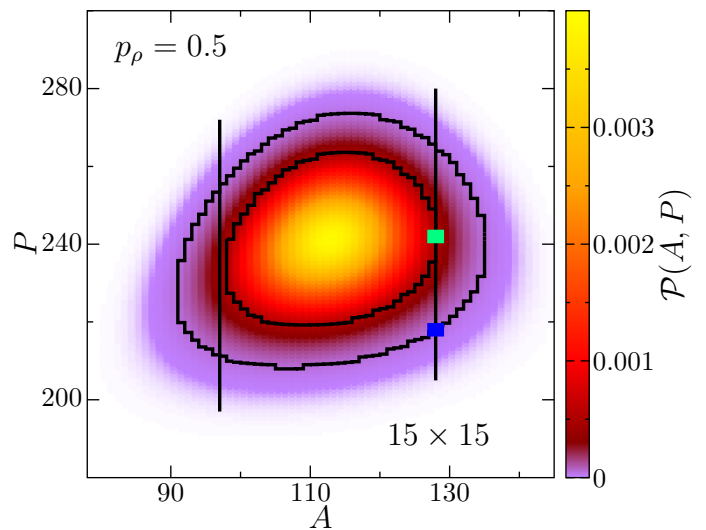


Fig. 3. Probability distribution \mathcal{P} of area A and perimeter P of a 15×15 b/w image with probability $p_\rho = 0.5$ for a pixel being black.

However, comparing $\mathcal{D}(A)$ to $\mathcal{D}(A, P, \chi)$, there is no additional information in the perimeter P or Euler characteristic χ : If there is only a single black pixel at high thresholds, the only possible values for P and χ are 4 or 1, respectively. Therefore, the simple and joint deviation strengths are exactly identical.

For the uniform source, the additional information (P, χ) must, as stated above, lead to a decrease of the deviation strength. Interestingly, this decrease turns out to be rather small even in the extreme case of a constant offset. The decrease of the deviation strength could even be an advantage in that the joint deviation strength is slightly less sensitive to errors in the estimation of the background intensity and a source would still be detected because of the strong deviation in the area A .

For the structured source, there is a tremendous increase in sensitivity for the joint deviation strength compared to the simple one. For all counts maps for which the corresponding values of the deviation strengths are within the dashed box, the source is not detected if only the area characterizes the structure, but it is detected by the joint deviation strength, i.e., if all Minkowski functionals characterize the shape of the counts map. For the same counts map for which the simple deviation strength based only on the area is below 5, i.e., the compatibility is more than 10^{-5} , the joint deviation strength reaches values nearly 20, i.e., with compatibilities less than 10^{-19} . In other words, if the structure is characterized not only by the area but by all Minkowski functionals, the compatibility with the background structure can drop by 14 orders of magnitude. There is no significant excess in the total number of counts but in the structure of the counts map. Only by taking this morphometric information into account, a formerly undetected source can now be detected using the same data.

A more formal explanation of this intuitive understanding can be given with the aid of Fig. 3. Given a measured area, e.g., $A = 128$, the compatibility $\mathcal{C}(A)$ w.r.t. only the area is the sum over all probabilities left of the left dotted line and right of the right dotted line, i.e., all macrostates with an area less likely than the given area $A = 128$.

In the example of a uniform offset in the background intensity, the structure, quantified by the perimeter² P , is in agreement with the background structure and the perimeter most likely takes on a “typical” value, i.e., a likely perimeter for a given area A , e.g., the green square represents $P = 242$. The compatibility $C(A, P)$ is then the sum over all probabilities outside the inner contour line, which results in $C(A, P) > C(A)$. However, in the example of a structured source the perimeter P might take on an unlikely value for the perimeter, e.g., the blue square represents $P = 218$. The compatibility $C(A, P)$ is now the sum over all probabilities outside the outer contour line and thus, $C(A, P) < C(A)$. A structural deviation from the background structure leads to a more significant result of the morphometric analysis compared to simple counting methods. For two different b/w images with the same compatibility with the background w.r.t. the area, the additional information of the perimeter specifies whether the b/w image is indeed compatible to the background structure or not.

4. Comparison to a standard counting method

The standard null hypothesis test in gamma-ray astronomy was introduced in Li & Ma (1983): it compares the number of signals N_{on} in the so-called “on-region”, i.e., in the vicinity of an expected source, to the number of background signals detected in an N_{off} “off-region”, i.e., a region in the sky without sources. The method simply counts the number of photons. Given an exposure ratio α , the significance σ is

$$\sigma = \sqrt{\ln \left\{ \left[\frac{1 + \alpha}{\alpha} \left(\frac{N_{on}}{N_{on} + N_{off}} \right) \right]^{2N_{on}} \left[(1 + \alpha) \left(\frac{N_{off}}{N_{on} + N_{off}} \right) \right]^{2N_{off}} \right\}} \quad (3)$$

The significance can be expressed in terms of a deviation strength (Göring et al. 2013):

$$\mathcal{D}(\sigma) = -\log_{10} \left(\operatorname{erfc} \left(\frac{\sigma}{\sqrt{2}} \right) \right) \quad (4)$$

where $\operatorname{erfc}(x) = \frac{2}{\sqrt{\pi}} \int_x^\infty \exp(-t^2) dt$ is the error function. This standard counting method allows for a simple and fast null hypothesis test. However, the analysis only uses the total number of counts in the observation window.

Our morphometric analysis follows a completely new ansatz based on structure characterization, which can not only detect an excess of counts but is able to detect any structural deviation from the background noise. It can detect structural deviations in count maps where the number of expected counts is in perfect agreement with the background intensity (Klatt 2016).

4.1. Dependence on experimental details

Therefore, there is no direct and straightforward comparison that one of the methods is always more sensitive than the other. A comparison of the advantages and different possibilities of the two methods is complicated and depends on the experimental details and the source shape.

² Because of the white boundary conditions the perimeter can only take on even values; for an odd value of P the probability is zero. For an easier visualization the bin length in P is two.

The standard counting method is more likely to detect sources if there is no interesting structure to be quantified within the scan window. The additional structural information is in agreement with the background noise, as discussed in Section 3.2. The morphometric analysis based on all Minkowski functionals is, in this case, less likely to detect a source compared to an analysis that only takes the total number of counts into account. However, if there is a distinct structural difference from the background noise, the morphometric analysis has the advantage of being able to use this additional information.

Whether or not there is an increase in sensitivity compared to the counting method by Li and Ma also strongly depends on the experimental details, e.g., the bin size, as shortly discussed in Göring (2012). In contrast to the total number of counts, our morphometric analysis strongly depends on the choice of the bin size. If the bins are too large, interesting source structure might be hidden because it is contained in a single bin. However, if the bin size is too small, the sky map does not only get very noisy but we can also lose structural information. In the extreme case that in the black and white image all black pixels are separated from each other by white pixels, the translation invariant Minkowski functionals can no longer distinguish different configurations, but only the total number of black bins. Therefore, the bin size needs to be chosen reasonably taking the size of the scan window, the point spread function of the telescope, the quality of the data, and the source shape into account, see Göring (2012).

As mentioned above, the morphometric analysis can detect sources even if there is no excess in the signals compared to the background intensity, see Section 3.2. Therefore, we expect the morphometric analysis to be robust against overestimates of the background intensity λ . However, a more thorough analysis of such effects for real data is beyond the scope of this article. Ideally, it would need extensive simulations to determine the empirical cumulative distribution function with a priori unknown λ , but instead using an efficient estimation of the background intensity, as described in Göring (2012). A main advantage of the morphometric analysis compared to the counting method could eventually be that it avoids observations of off-region because a less precise estimate of the background intensity is sufficient.

The method by Li and Ma compares the number of counts in the source region and in regions with only background signals. Obviously, it strongly depends on how accurate the estimate of the background intensity is. Here, we compare the morphometric analysis to the significance of the Li and Ma test for the extreme and most sensitive case of an infinitely long observation of the off-region³ $N_{off} \rightarrow \infty$ while $\alpha = \lambda_{tot}/N_{off} \rightarrow 0$. In this limit,

$$\sigma = \sqrt{2} \left\{ N_{on} \ln \left[\frac{N_{on}}{\lambda_{tot}} \right] + \lambda_{tot} - N_{on} \right\}^{1/2} \quad (5)$$

For a final comparison of both methods, their dependencies on these experimental details must be accurately studied, which is beyond the scope of this article. Here, we discuss the advantages of the refined morphometric analysis and compare it to the counting method in two examples,

³ An infinite observation time corresponds to using the exact background intensity.

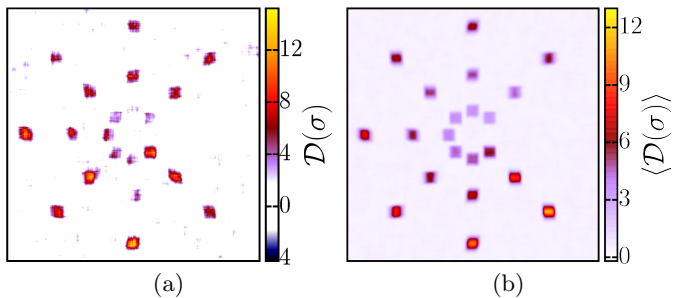


Fig. 4. For the test pattern in Fig. 1, the excess in the total number of counts is determined; the deviation strength in the total number of counts is derived from the significance of the excess according to Eqs. (4) and (5): (a) a single sky map is shown like in Figs. 1(b) or 1(c), (b) an average of 100 Minkowski sky maps like in Figs. 1(d) or 1(e); for a direct comparison, the same color scales are used. For the chosen 15×15 scan window, the outer sources are detected with a similar significance as in Fig. 1. However, in order to detect the inner sources, the scan window size must be adjusted.

where the morphometric analysis detects sources in contrast to the standard method by Li and Ma. These examples show the potential of the morphometric ansatz. However, the choice of the optimal method strongly depends on the details of the data which is to be analyzed, as well as, on the information or features that are to be extracted.

4.2. Scan window size dependence and low statistics

Besides the above mentioned robustness against overestimated background intensities or the ability to even detect inhomogeneities with no excess in the total number of counts, another important advantage of the morphometric analysis is that it depends much less on the choice of the size of the scan window. Even sources with extensions much smaller than the scan window size are detected in the morphometric analysis, although there is no significant change in the total number of counts.

Figure 2 shows how even a point source, i.e., a single pixel with increased intensity, can sensitively be detected, because at high threshold even a single black pixel is very unlikely, which is independent of counts in other pixels possibly in agreement with the null hypothesis. The morphometric analysis can detect sources of very different extensions with the same scan window size.

In contrast to this, the standard counting method cannot detect a source if there are at the same time too many pixels with only background signals in the same scan window. If there are many pixels within the scan window which contain only background signals, the source signals can be suppressed. The small excess in the total number of counts is no longer significant. This effect can be reduced if the size of the scan window is adjusted to the extension of the source. However, such an adaption can possibly lead to a biased choice of the parameter or an unknown trial factor if the analysis is repeated with different window size.

In Fig. 4, the test pattern from Fig. 1 with differently large sources is analyzed using the same scan window size as the morphometric analysis, see Figs. 1(b)–1(e). The large

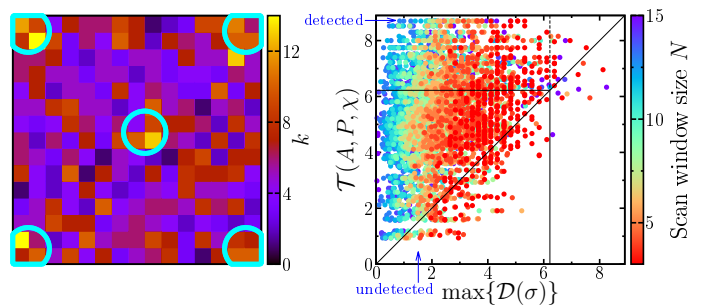


Fig. 5. A source like a dotted pattern where only low statistics are available: (a) the source consists of several point-like sources (marked by circles) hardly visible by eye in the counts map; (b) comparison of the deviation strength $\mathcal{T}(A, P, \chi)$ of the morphometric analysis to $\mathcal{D}(\sigma)$ of the standard counting method from Eqs. (4) and Eq. (5). 400 samples are simulated. For each sample, the morphometric analysis is applied to the whole 15×15 counts map. For the same sample, it is compared to $\mathcal{D}(\sigma)$, which is evaluated for all scan window sizes between 15×15 (blue points) and 3×3 (red points) where the maximum of all iterations over the counts map is used. Although the trial factors for $\max\{\mathcal{D}(\sigma)\}$ are ignored, the morphometric analysis is for the vast majority of samples more sensitive $\mathcal{T}(A, P, \chi) > \max\{\mathcal{D}(\sigma)\}$. Although there might be no significant excess in the total number of counts, the source can be detected by taking more information out of the same data.

outer sources are of the same size as the scan window; they are detected with a similar significance as by the morphometric analysis. However, the smaller inner sources are not statistically significantly detected, because there are too many background signals in the same scan window. If the scan window size is adjusted, these sources can be detected highly significantly. However, the problem of a possibly biased choice of parameters, as well as, an unknown trial factor remains.

The most important advantage of the morphometric analysis is, of course, that it incorporates additional structural information. Especially, if only low statistics are available, an increase in the sensitivity by quantifying the structure of the counts map is probably most needed. For example, a slight excess in the total number of counts might not be significant because of the strong fluctuations of a Poisson distribution relative to the small mean value. Interestingly, especially in such a case the significance in the structural deviation is relatively strong compared to the significance in the number of counts. For example, for a Poisson random field with a low intensity the clustering of a given number of black pixels is equally likely or unlikely as in a field with high intensity. The excess in the number of counts might not be significant, but the improbable arrangement of the black pixels can lead to the detection of the source. So, the advantage of additional structural information should be most effective when it is most needed.

Figure 5 shows such an example of a weak and hardly detectable source where only low statistics are available. Although hardly visible by eye in the count map, there are strong intensity gradients. The source resembles a dotted pattern; it consists of several nearly pointlike sources that are marked in the count map on the left-hand side. Because of the strong intensity gradients and thus the sig-

nificant structural deviation from the background noise, the morphometric analysis can take advantage of the additional geometrical information.

Because of the low statistics, there are strong statistical fluctuations in the single sky maps. We therefore do here not use the maximal deviation strength over all thresholds, but an improved test statistic that combines the deviations strength of different thresholds, as explained in the Appendix A. For a more systematic analysis, I simulate 400 samples and compare the deviation strength $\mathcal{T}(A, P, \chi)$ of the morphometric analysis to $\mathcal{D}(\sigma)$ of the standard counting method from Eqs. (4) and (5), see the right-hand side of Fig. 5.

The morphometric analysis analyzes the whole 15×15 count map. However, it is not only compared to $\mathcal{D}(\sigma)$ of the standard counting method using the same scan window size (blue points), rather for all scan windows down to very small sizes 3×3 (red points). Thus, the effect of windows size dependence in the standard counting method can be taken into account. For scan windows smaller than the total size of the counts map, we iterate the scan window over the count map and compare the maximum of all deviation strengths $\mathcal{D}(\sigma)$ to $\mathcal{T}(A, P, \chi)$.

Although the thus necessary trial factors for $\max\{\mathcal{D}(\sigma)\}$ are ignored, which in some cases would reduce the deviation strength by more the 1.4, the morphometric analysis is for the vast majority of samples more sensitive than the counting method $\mathcal{T}(A, P, \chi) > \max\{\mathcal{D}(\sigma)\}$. While there are only about 5 out of 400 samples with $\max\{\mathcal{D}(\sigma)\} > 6.22$, there are many samples where the source is not detected by $\max\{\mathcal{D}(\sigma)\}$ but by $\mathcal{T}(A, P, \chi)$. In other words, although there might be no significant excess in the total number of counts, the source can still be detected by taking more information out of the same data. In general, a comparison of the morphometric analysis and the standard method by Li and Ma depends on both the experimental details and the structure of the source. For this example, the morphometric analysis is more sensitive.

5. Conclusion

The morphometric analysis allows to detect gamma-ray sources via structural deviations from the background noise without any assumptions about potential sources.

Comparing the simple to the joint structure characterization, we can demonstrate a significant increase in sensitivity due to the additional shape information that is extracted from the data, see Fig. 1. For the same counts map for which the simple deviation strength based only on the area is below 5, i.e., the compatibility is more than 10^{-5} , the joint deviation strength can reach values of nearly 20, i.e., compatibilities less than 10^{-19} , see Fig. 2. The compatibility with the background structure drops by 14 orders of magnitude and formerly undetected sources can be detected simply by applying a refined morphometric analysis. Of course, the increase in sensitivity depends on the shape of the source, see Fig. 3.

A comparison of the morphometric analysis to the standard null hypothesis test by Li and Ma in gamma-ray astronomy, see Eqs. (4) and (5), depends both on the shape of the source and on the experimental details, like the binning or the accuracy of the estimate of the background intensity. The morphometric analysis follows a very different ansatz.

Besides the advantage of including additional structural information, it depends less on the size of the scan window and can detect both rather extended and pointlike sources using the same scan window size, compare Figs. 1 and 4. Moreover, the advantage of additional structural information should be most effective for short observation times and low statistics. Figure 5 shows an example for which there is no significant excess in the total number of counts, but the source can still be detected because of the additional structural information.

In summary, the main advantages of the morphometric analysis are:

- a shape analysis without prior knowledge about potential sources,
- a sensitivity gain via structure information especially for low statistics,
- its relative independence of the scan window size, and
- its detection of statistically significant inhomogeneities in the counts map even if the expected total number of counts is in perfect agreement with the background intensity.

Moreover, we expect for the reasons discussed above that it is robust against errors in the estimation of the background intensity.

The simulation study in this article, demonstrates how additional information extracted from the same data can allow the detection of formerly undetected sources. The next step is to apply these improved techniques to real data from experiments; for first examples of applications to H.E.S.S. sky maps, see Göring (2008, 2012); Klatt (2016).

6. Outlook

The morphometric analysis is here shown to be an innovative and efficient spatial data analysis. Of course, there are even further possibilities to extend the analysis. For example, the method can naturally be extended to any spatial dimension if the structure of the D dimensional b/w image is characterized by the $(D + 1)$ Minkowski functionals.

6.1. Other shape descriptors

The above-defined analysis is very general, and indeed any useful shape descriptor can be used. The Minkowski functionals are versatile tools and can comprehensively quantify the structure of quite different random fields. However, if for a certain system another index is better physically motivate, more important or interesting, it can replace the Minkowski functionals, but the basic idea remains unchanged. Only the probability distribution, i.e., the DoS has to be determined following the procedure from the second paper in this series.

The Minkowski functionals already incorporate all additive and conditional continuous scalar geometrical information, and we have already also introduced the Minkowski tensors to the morphometric analysis in Klatt (2010). Other shape descriptors like the convexity number (Stoyan et al. 1987) or Betti numbers (Robins 2002) are directly applicable to the method describe above, but the calculations will be more time consuming.

Even functions can be used as shape characteristics. A first example could be the cluster function that is the probability of finding two points at a given distance in the same

cluster. Only one additional step is needed: the correlation function must be mapped to a scalar. A good choice would be the integral over the absolute value of the difference to the mean value (i.e., expected) correlation function of a Poisson random field; this is well defined if there are no long-range correlations, because then all correlation functions converge sufficiently fast to the same constant and thus, the difference to zero. An even more interesting example could be correlation functions of Minkowski functionals (Mecke et al. 1994; Klatt & Torquato 2014).

6.2. Further random fields

We have developed the morphometric analysis for analyzing counts map in gamma-ray astronomy, where the counts in different pixels are uncorrelated because they result from different events (showers) clearly separated in time. We here show how the morphometric analysis distinguishes homogeneous from inhomogeneous Poisson random fields. However, the morphometric analysis allows for a much more general analysis. It can detect other deviations from a Poisson assumption, e.g., correlations between the counts in different pixels; see Section 6.2. There might be no deviation in the number of counts (globally or even locally), but a strong deviation in the structure quantified by the Minkowski functionals.

Although we have developed the morphometric analysis for analyzing counts map with uncorrelated pixels, its use might even be more efficient for other applications with correlations between the counts in different pixels, for example, in detectors where an event is simultaneously triggered in neighboring pixels.

Note also, that the concept of the morphometric analysis can immediately be extended to other random fields, e.g., the Boolean models or the Gaussian random field. The Minkowski functionals are, as mentioned above, already used to search for statistical significant deviations from a Gaussian random field in the cosmic microwave background; for example, see (Schmalzing et al. 1999; Gay et al. 2012; Ducout et al. 2013). Of course, the probability distributions of the Minkowski functionals need to be determined and probably only numerical estimates are possible.

6.3. Extensions of the test statistic

In the appendix, we introduce a new test statistic combining different thresholds, see Eq. (A.2). Instead of the maximum of the deviation strength, we use the sum of the deviation strengths over all thresholds, see Eq. (A.1). We determine the empirical complementary cumulative distribution function, see Fig. A.1. The combination of the structural information at different thresholds improves especially the detection of diffuse radiation and extended sources, see Fig. A.3.

Acknowledgements. We thank Christian Stegmann and Daniel Göring for valuable discussions, suggestions, and advice. We thank the German Research Foundation (DFG) for the Grant No. ME1361/11 awarded as part of the DFG-Forschergruppe FOR 1548 “Geometry and Physics of Spatial Random Systems.”

Appendix A: Combining different thresholds

So far, only the deviation strength of a single threshold is directly used for the null hypothesis test. The deviation

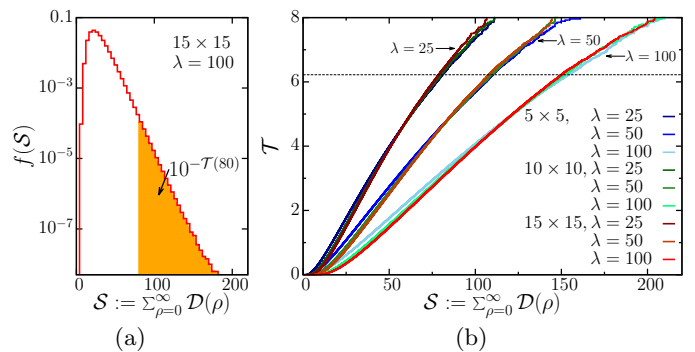


Fig. A.1. Sum of deviation strengths $\mathcal{D}(\rho)$ over all thresholds ρ : (a) empirical probability density function $f(\mathcal{S})$ and (b) the new test statistic \mathcal{T} , which is the negative decadic logarithm of the empirical complementary cumulative distribution function for different system sizes and background intensities λ ; the dashed line indicates the hypothesis criterion, which is adjusted to the common 5σ criterion.

strengths at other thresholds are used only indirectly by the fact that they are smaller than the maximum. However, the deviation strength as a function of the thresholds contains a lot of information, e.g., even to some degree the extension of the source (Göring et al. 2013, Fig. 3). Taking this information into account could yield a profound additional insight in the spatial data. However, it is currently out of reach to determine the probability distribution of the deviation strength as a function of the threshold.

Nevertheless, the most important information is whether the maximal deviation strength is only a fluctuation at a single threshold or whether there are strong structural deviations over a large range of thresholds (Göring et al. 2013, Fig. 3). This can be quantified by replacing the maximum of the deviation strength by the sum of all thresholds⁴,

$$\mathcal{S} := \sum_{\rho=0}^{\infty} \mathcal{D}(\rho), \quad (\text{A.1})$$

which is well defined, i.e., $\mathcal{S} < \infty$, because for every counts map there is a maximum count k_{\max} ; thus, for $\rho > k_{\max}$ the b/w image is completely white. For a large enough threshold $\rho_l \gg 1$, this becomes the most likely configuration, because if $p \rightarrow 0$, $\mathcal{P}(A = 0) = (1 - p)^{N^2} \rightarrow 1$. For $\rho > \rho_l$, the compatibility is one and the deviation strength zero; the series, defined in Eq. (A.1), is actually a finite sum.

The sum \mathcal{S} is a new test statistic instead of the maximum deviation strength \mathcal{D} before. The distribution of this new test statistic can be calculated analytically, but efficient and tight approximations might be achievable, although out of the scope of this article. Here, the cumulative distribution is determined numerically, and the sensitivity gain is shown for simulated data.

A.1. Empirical cumulative distributions

We simulate 10^9 counts maps and for each calculate $\mathcal{S} := \sum_{\rho=0}^{\infty} \mathcal{D}(\rho)$, from which I derive the Empirical Probability Density Function (EPDF) for different window sizes and

⁴ The infinity norm l_{∞} is replaced by the 1-norm l_1 .

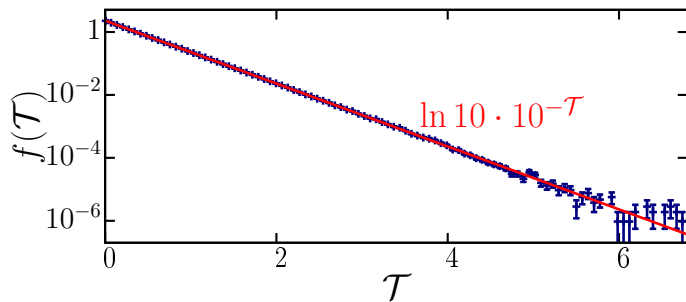


Fig. A.2. Empirical probability density function of the test statistic \mathcal{T} from Eq. (A.2) for a 15×15 count map with a background intensity $\lambda = 50$; it is in very good agreement with the target probability distribution from Eq. (A.3).

background intensities. Figure A.1 shows the EPDF $f(\mathcal{S})$ for a 15×15 Poisson counts map with intensity $\lambda = 100$.

The new test statistic is defined as the empirical complementary cumulative distribution function (ECCDF), i.e., given a measured sum of deviation strength \mathcal{S} , the probability to find a larger value $\mathcal{S}' > \mathcal{S}$. This definition follows, as that for the compatibility C in Section 2, the scheme given in Neyman & Pearson (1933) to construct a most efficient hypothesis test.

For convenience, again the negative decadic logarithm is used instead,

$$\mathcal{T}(\mathcal{S}) = -\log_{10} \int_{\mathcal{S}}^{\infty} ds f(\mathcal{S}), \quad (\text{A.2})$$

and the null hypothesis is rejected if $\mathcal{T} > 6.2$, which corresponds to the common 5σ criterion. Figure A.1 plots Eq. (A.2) for different system sizes and background intensities, based on 10^9 simulated count maps for each system.

As expected, the test statistic strongly depends on the background intensity λ because the number of thresholds with nonzero deviation strength varies. Interestingly, the dependence on the system size is rather weak.

The new test statistic is chosen such that in simulations of the background model, its EPDF is the same as for the deviation strength \mathcal{D} at a single threshold,

$$f(\mathcal{T}) = \ln 10 \cdot 10^{-\mathcal{T}}, \quad (\text{A.3})$$

see Fig. A.2.

A.2. Sensitivity increase for diffuse radiation

Especially for broad sources, which exhibit structural deviations at a large range of thresholds, the new test statistic \mathcal{T} can lead to an additional increase in sensitivity.

Figure A.3 exemplarily shows this increase for simulated diffusion radiation. The new testing procedure is more sensitive because it includes the information that there are also strong structural deviations at other thresholds than the maximum deviation strength.

References

Aharonian, F. et al. 2006a, *Astron. Astrophys.*, 449, 223
Aharonian, F. et al. 2006b, *Nature*, 439, 695
Aharonian, F. et al. 2007, *Astrophys. J.*, 661, 236
Arfelli, F. et al. 2000, *Radiology*, 215, 286
Atwood, W. B. et al. 2009, *Astrophys. J.*, 697, 1071

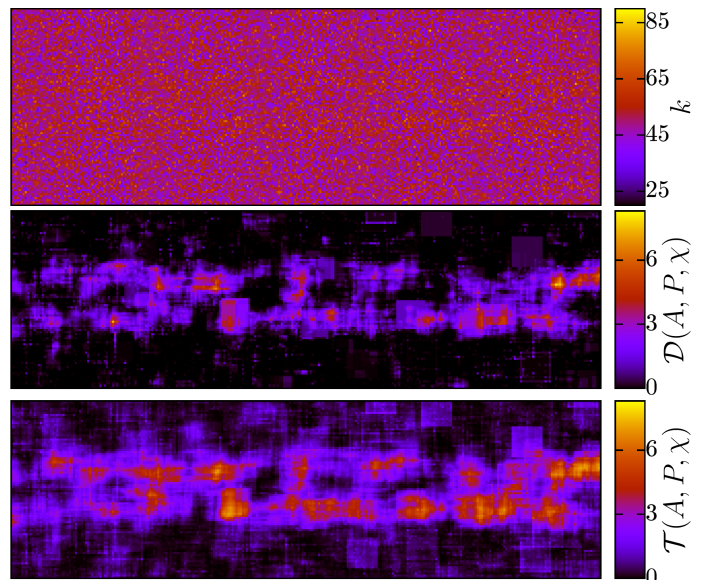


Fig. A.3. Diffuse radiation along the horizontal axis is added to a homogeneous background noise with intensity $\lambda = 50$, which leads to an excess in the number of counts k (top). The Minkowski sky map based on the maximum of the deviation strength \mathcal{D} w.r.t. all Minkowski functionals detects the structural deviations of this very broad source (center), but the new test statistic that sums over all thresholds leads to a significant increase in sensitivity (bottom).

Borg, M., Thirde, D., Ferryman, J., et al. 2005, in *Advanced Video and Signal Based Surveillance, 2005. AVSS 2005. IEEE Conference on*, 16
Buckley, J., Byrum, K., Dingus, B., et al. 2008, *ArXiv e-prints*, arXiv:0810.0444
Canuto, H. C., McLachlan, C., Kettunen, M. I., et al. 2009, *Magn. Reson. Med.*, 61, 1218
Colombi, S., Pogossyan, D., & Souradeep, T. 2000, *Phys. Rev. Lett.*, 85, 5515
Ducout, A., Bouchet, F. R., Colombi, S., Pogossyan, D., & Prunet, S. 2013, *Mon. Not. R. Astron. Soc.*, 429, 2104
Gay, C., Pichon, C., & Pogossyan, D. 2012, *Phys. Rev. D*, 85, 023011
Göring, D. 2008, Master's thesis (Diplomarbeit), Universität Erlangen-Nürnberg
Göring, D. 2012, *Gamma-Ray Astronomy Data Analysis Framework based on the Quantification of Background Morphologies using Minkowski Tensors*, PhD thesis, Universität Erlangen-Nürnberg
Göring, D., Klatt, M. A., Stegmann, C., & Mecke, K. 2013, *Astron. Astrophys.*, 555, A38
Jain, A. K., Duin, R. P. W., & Mao, J. 2000, *IEEE T. Pattern Anal.*, 22, 4
Kerscher, M., Mecke, K., Schmalzing, J., et al. 2001, *Astron. Astrophys.*, 373, 1
Klatt, M. A. 2010, Master's thesis (Diplomarbeit), Universität Erlangen-Nürnberg
Klatt, M. A. 2016, *Morphometry of random spatial structures in physics*, PhD thesis, Friedrich-Alexander-Universität Erlangen-Nürnberg (FAU).
Klatt, M. A., Göring, D., Stegmann, C., & Mecke, K. 2012, *AIP Conf. Proc.*, 1505, 737
Klatt, M. A. & Torquato, S. 2014, *Phys. Rev. E*, 90, 052120
Larkin, T. J., Canuto, H. C., Kettunen, M. I., et al. 2014, *Magn. Reson. Med.*, 71, 402
Li, T.-P. & Ma, Y.-Q. 1983, *Astrophys. J.*, 272, 317
M. Kerscher, K. Mecke, P. Schuecker, et al. 2001, *Astron. Astrophys.*, 377, 1
Mantz, H., Jacobs, K., & Mecke, K. 2008, *J. Stat. Mech.*, 12, P12015
Mattox, J. R. et al. 1996, *Astrophys. J.*, 461, 396
Mecke, K., Buchert, T., & Wagner, H. 1994, *Astron. Astrophys.*, 288, 697
Michel, T. et al. 2013, *Phys. Med. Biol.*, 58, 2713

- Neyman, J. & Pearson, E. S. 1933, *Phil. Trans. R. Soc. London, Ser. A*, 231, 289
- Novaes, C., Bernui, A., Ferreira, I., & Wuensche, C. 2014, *J. Cosmol. Astropart. Phys.*, 2014, 018
- Novikov, D., Schmalzing, J., & Mukhanov, V. F. 2000, *Astron. Astrophys.*, 364, 17
- Quast, K. & Kaup, A. 2011, *EURASIP J. Image Video Process.*, 2011, 14
- Robins, V. 2002, in *Lecture Notes in Physics, Vol. 600, Morphology of Condensed Matter*, ed. K. Mecke & D. Stoyan (Springer, Berlin, Heidelberg), 261
- Schmalzing, J., Buchert, T., Melott, A. L., et al. 1999, *Astrophys. J.*, 526, 568
- Schneider, R. & Weil, W. 2008, *Stochastic and Integral Geometry (Probability and Its Applications)* (Berlin: Springer)
- Schröder-Turk, G. E., Kapfer, S., Breidenbach, B., Beisbart, C., & Mecke, K. 2010, *J. Microsc.*, 238, 57
- Schröder-Turk, G. E., Mickel, W., Kapfer, S. C., et al. 2011, *Adv. Mater.*, 23, 2535
- Schröder-Turk, G. E., Mickel, W., Kapfer, S. C., et al. 2013, *New J. Phys.*, 15, 083028
- Schuetrumpf, B., Klatt, M. A., Iida, K., et al. 2013, *Phys. Rev. C*, 87, 055805
- Schuetrumpf, B., Klatt, M. A., Iida, K., et al. 2015, *Phys. Rev. C*, 91, 025801
- Stonebraker, M., Frew, J., Gardels, K., & Meredith, J. 1993, *SIGMOD Rec.*, 22, 2
- Stoyan, D., Kendall, W., & Mecke, J. 1987, *Stochastic geometry and its applications* (John Wiley and Sons)
- Theodoridis, S. & Koutroumbas, K. 2009, *Pattern Recognition*, 4th edn. (Boston: Academic Press)
- Wiegand, A., Buchert, T., & Ostermann, M. 2014, *Mon. Not. R. Astron. Soc.*, 443, 241
- Yilmaz, A., Javed, O., & Shah, M. 2006, *ACM Comput. Surv.*, 38